Article

Composition Control and Localization of S in CdSSe Quantum Dots Grown from Li[CdSe(SPh)]

Derek D. Lovingood, Ryan E. Oyler, and Geoffrey F. Strouse

J. Am. Chem. Soc., **2008**, 130 (50), 17004-17011 • DOI: 10.1021/ja805453s • Publication Date (Web): 17 November 2008

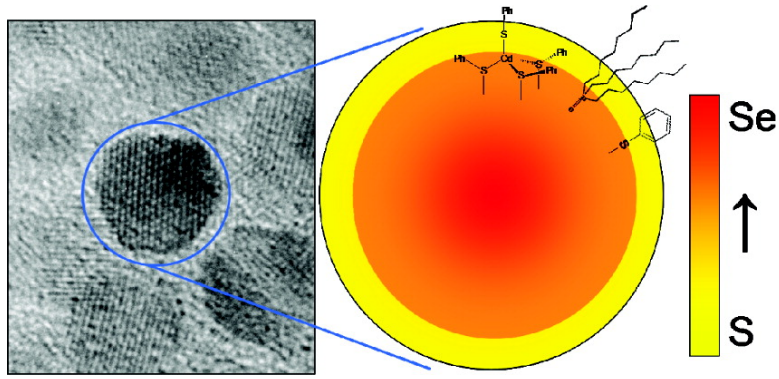

More About This Article

Additional resources and features associated with this article are available within the HTML version:

- Supporting Information
- Access to high resolution figures
- Links to articles and content related to this article
- Copyright permission to reproduce figures and/or text from this article

View the Full Text HTML

J|A|C|S
ARTICLES

Published on Web 11/17/2008

Composition Control and Localization of S^{2-} in CdSSe Quantum Dots Grown from $Li_4[Cd_{10}Se_4(SPh)_{16}]$

Derek D. Lovingood, Ryan E. Oyler, and Geoffrey F. Strouse*

Department of Chemistry and Biochemistry, Florida State University, Tallahassee, Florida 32306-4390

Received July 14, 2008; E-mail: strouse@chem.fsu.edu

Abstract: The development of ternary nanoscale materials with controlled cross-sectional doping is an important step for the use of chemically prepared quantum dots for nanoscale engineering applications. We report cross-sectional, elemental doping with the formation of an alloyed CdSSe nanocrystal from the thermal decomposition of $Li_4[Cd_{10}Se_4(SPh)_{16}]$. The sulfur incorporation arises from surface-mediated phenylthiolate degradation on the growing quantum dot surface. In the alloy, we identify a pure CdSe nucleus of ~1.5 nm, consistent with the predictions of nucleation theory. As the particle grows, S^{2-} incorporation increases until the CdSSe reaches ~4 nm, where a marked reduction in phenylthiolate content on the nanocrystal is observed by CP-MAS NMR spectroscopy, implying that rapid decomposition of the phenylthiolate arises with subsequent enhanced S^{2-} incorporation at the level of the stoichiometry of the reaction (namely ~60%). The use of molecular clusters to allow controlled defect ion incorporation can open new pathways to more complex nanomaterials.

Introduction

Preparation of emissive quantum dots (QDs) has evolved to the point where very narrow size dispersions of the desired binary or ternary semiconductor can be prepared routinely, whether through the use of molecular reactants,[1−3] single-source, dual-component precursors,[4] or single-source inorganic clusters.[5−8] The growth of the II−VI QDs from inorganic clusters, while well documented,[11−27] is mechanistically poorly understood. Depending on the reaction temperature and conditions, we[8] and others[10] have observed variable concentrations of S^{2-} incorporation into CdSe QDs grown from $[Cd_{10}Se_4(SPh)_{16}]^{4-}$, the parentage of which can be traced to phenylthiolate decomposition at the QD surface. Incorporation of S^{2-} is not surprising based on earlier studies by Wang and Herron for CdS formation from the cluster $[Cd_{10}S_4(SPh)_{16}]^{4-}$, where 60% of the S^{2-} incorporation came from phenylthiolate ligand decomposition.[28] They observed a surface-mediated cleavage reaction between two bridging SPh^- groups with ensuing production of S^{2-} and loss of diphenyl sulfide. Extrapolation of these results to the growth of QDs from $[Cd_{10}Se_4(SPh)_{16}]^{4-}$ would suggest a CdSSe alloy with a composition approaching 60% S^{2-} might be expected based on stoichiometry. However, the rate of incorporation would be influenced by the rate of decomposition of the phenylthiolate, which is both temperature dependent and surface area dependent on the growing QD.

(1) Murray, C. B.; Noms, D. J.; Bawendi, M. G. *J. Am. Chem. Soc.* **1993**, *115*, 8706–8715.
(2) Peng, Z. A.; Peng, X. G. *J. Am. Chem. Soc.* **2001**, *123*, 1389–1395.
(3) Swafford, L. A.; Weigand, L. A.; Bowers, M. J., II; McBride, J. R.; Rapaport, J. L.; Watt, T. L.; Dixit, S. K.; Feldman, L. C.; Rosenthal, S. J. *J. Am. Chem. Soc.* **2006**, *128*, 12299–12306.
(4) Ludolph, B.; Malik, M. A.; O'Brien, P.; Revaprasadu, N. *Chem. Commun.* **1998**, *1849*, 1850.
(5) Cumberland, S. L.; Hanif, K. M.; Javier, A.; Khitrov, G. A.; Strouse, G. F.; Woessner, S. M.; Yun, C. S. *Chem. Mater.* **2002**, *14*, 1576–1584.
(6) Trindade, T.; O'Brien, P.; Zhang, X. M. *Chem. Mater.* **1997**, *9*, 523–530.
(7) Nair, P. S.; Scholes, G. D. *J. Mater. Chem.* **2006**, *16*, 467–473.
(8) Magana, D.; Wei, X.; Strouse, G. F. *Phys. Rev. B* **2008**, *77*, 115337.
(9) Archer, P. I.; Santangelo, S. A.; Gamelin, D. R. *Nano Lett.* **2007**, *7*, 1037–1043.
(10) Archer, P. I.; Santangelo, S. A.; Gamelin, D. R. *J. Am. Chem. Soc.* **2007**, *129*, 9808–9818.
(11) Aslam, F.; Stevenson-Hill, J.; Binks, D. J.; Daniels, S.; Pickett, N. L.; O'Brien, P. *Chem. Phys.* **2007**, *334*, 45–52.
(12) Li, Y.; Feng, J.; Daniels, S.; Pickett, N. L.; O'Brien, P. *J. Nanosci. Nanotechnol.* **2007**, *7*, 2301–2308.
(13) Magana, D.; Perera, S. C.; Harter, A. G.; Dalal, N. S.; Strouse, G. F. *J. Am. Chem. Soc.* **2006**, *128*, 2931–2939.
(14) Gerbec, J. A.; Magana, D.; Washington, A.; Strouse, G. F. *J. Am. Chem. Soc.* **2005**, *127*, 15791–15800.
(15) Javier, A.; Meulenberg, R. W.; Yun, C. S.; Strouse, G. F. *J. Phys. Chem. B* **2005**, *109*, 6999–7006.
(16) Meulenberg, R. W.; Jennings, T.; Strouse, G. F. *Phys. Rev. B* **2004**, *70*, 235311.
(17) Meulenberg, R. W.; van Buuren, T.; Hanif, K. M.; Willey, T. M.; Strouse, G. F.; Terminello, L. J. *Nano Lett.* **2004**, *4*, 2277–2285.
(18) Javier, A.; Strouse, G. F. *Chem. Phys. Lett.* **2004**, *391*, 60–63.
(19) Berrettini, M. G.; Braun, G.; Hu, J. G.; Strouse, G. F. *J. Am. Chem. Soc.* **2004**, *126*, 7063–7070.
(20) Javier, A.; Magana, D.; Jennings, T.; Strouse, G. F. *Appl. Phys. Lett.* **2003**, *83*, 1423–1425.
(21) Aslam, F.; Binks, D. J.; Daniels, S.; Pickett, N.; O'Brien, P. *Chem. Phys.* **2005**, *316*, 171–177.
(22) Aslam, F.; Binks, D. J.; Rahn, M. D.; West, D. P.; O'Brien, P.; Pickett, N; Daniels, S. *J. Chem. Phys.* **2005**, *122*, 184713.
(23) Aslam, F.; Binks, D. J.; Rahn, M. D.; West, D. P.; O'Brien, P.; Pickett, N. *J. Mod. Opt.* **2005**, *52*, 945–953.
(24) Raola, O. E.; Strouse, G. F. *Nano Lett.* **2002**, *2*, 1443–1447.
(25) Hanif, K. M.; Meulenberg, R. W.; Strouse, G. F. *J. Am. Chem. Soc.* **2002**, *124*, 11495–11502.
(26) Meulenberg, R. W.; Strouse, G. F. *Phys. Rev. B* **2002**, *66*, 035317.
(27) Meulenberg, R. W.; Bryan, S.; Yun, C. S.; Strouse, G. F. *J. Phys. Chem. B* **2002**, *106*, 7774–7780.
(28) Farneth, W. E.; Herron, N.; Wang, Y. *Chem. Mater.* **1992**, *4*, 916–922.

10.1021/ja805453s CCC: $40.75

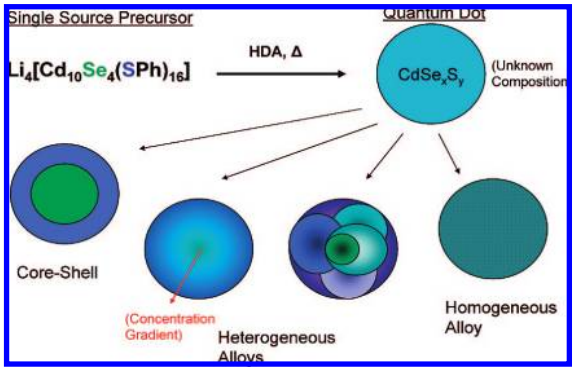

Figure 1. Possible composition scenarios for a CdSSe QD grown from the cluster $Li_4[Cd_{10}Se_4(SPh)_{16}]$.

In this solid solution, the anion distribution throughout the QD may exist as homogeneous, heterogeneous, gradient, or perhaps core−shell,[3,29] depending on the competition between phenylthiolate decomposition, phenylthiolate concentration, and rate of S^{2-} versus Se^{2-} addition to a growing QD surface (Figure 1). The possibility of a core−shell motif was first suggested by Gamelin et al.[10] due to the observation of enriched S^{2-} content at the QD surface. A core−shell motif is not necessary to observe enrichment of S^{2-} at the surface based on our NMR observation[30] of strongly bound SPh^- at the QD surface, which would result in the identical conclusion of S^{2-} enrichment but not imply a core−shell motif. The remarkable stability of the phenylthiolate at the surface (impervious to ligand exchange in pyridine) and the lack of detrimental effects on the quantum yield imply that the phenylthiolate anion exists either bound to the face or on unique vertex and edge sites, as suggested in our earlier study.[30] These results have prompted a more in-depth study into the quality of the resultant QD grown from the inorganic cluster source, the nature of the anion distribution in the solid solution, and the complexity associated with the incorporation of defect ions into a growing QD.

A CdSSe alloy is observed in the size regime greater than 1.5 nm, with a S^{2-} incorporation value of ∼60% for sizes in excess of 3.5 nm. The correlation of stoichiometry and microanalysis of the CdSSe alloy is remarkable but does not imply that the alloy is uniform over all size regimes. By correlating X-ray fluorescence (XRF), thermogravimetric analysis (TGA), solid-state NMR (SSNMR), UV−vis absorption, and powder X-ray diffraction (pXRD, size analysis), we demonstrate the formation of a CdSSe gradient as the QD grows. The size of the QDs in this study was calculated on the basis of Debeye−Scherrer analysis of the pXRD ⟨110⟩ face, which has been demonstrated to be valid for QD size estimation. The largest sizes were validated also by transmission electron microscopy (TEM). The optical absorption of the CdSSe materials shows a blue shift in the energy due to the increasing S^{2-} content, as predicted by the effective mass approximation for a ternary semiconductor. SSNMR analysis provides evidence of a combination of trioctylphosphine oxide (TOPO) and the phenylthiolate species passivating the CdSSe nanocrystals below 5 nm. Above 5 nm, no phenylthiolate contributions are observed, and the S^{2-} content in the nanocrystals reaches an asymptote in the XRF analysis. SSNMR correlated to XRF and effective mass approximation (EMA) studies lead us to conclude that anion distribution approaches the stoichiometric value of 60% for sulfur and 40% for selenium.

Experimental Section

Chemicals. The molecular clusters $Li_4[Cd_{10}Se_4(SPh)_{16}]$ and $Li_4[Cd_{10}Se_4(SePh)_{16}]$ were prepared as previously described.[31−33] Hexadecylamine (HDA, 90%), 85% H_3PO_4, and 12 M HCl were used without further purification.

Instrumentation. Elemental composition analysis for Cd^{2+}, S^{2-}, and Se^{2-} was carried out in an Oxford Instruments ED2000 X-ray fluorescence spectrometer with a Cu Kα source. The mole ratio for Cd^{2+} to Se^{2-} to S^{2-} for each sample was analyzed using XRF, with four repeat analyses for statistical validation. For a standard XRF measurement, the powdered samples were completely dissolved in 90% HNO_3 to allow total elemental composition to be analyzed. In order to allow compatibility with the XRF sample holder, the samples were heated to remove excess NO_x and then diluted to ∼5 mL with a 2% HNO_3 solution. All measurements were carried out at the Kα line for the element: Cd^{2+}, 23.1 keV; Se^{2-}, 11.2 keV; and S^{2-}, 2.3 keV. A total above 10 counts/s is needed to reduce error in the analysis. Calibration curves were generated using commercially prepared 1000 ppm elemental standards in 2% HNO_3, which results in accuracies of ±3 ppm for Cd^{2+}, ±4 ppm for Se^{2-}, and ±16 ppm for S^{2-}. Composition analyses of bulk samples were used to further validate the method.

Optical absorption was analyzed in a 1-cm cell in toluene (∼1 × 10^6 mol) using a Cary 50 UV−vis spectrophotometer. Powder X-ray diffraction was carried out on a Rigaku DMAX 300 Ultima 3 diffractometer using Cu Kα (λ = 1.5418 A) with the *d*-spacing calibrated to a Si^0 standard to verify crystal motif. Using the Debye−Scherrer formula (eq 1) the QD diameter was calculated,

$$\tau = \frac{K\lambda}{\beta \cos\theta} \quad (1)$$

where τ is the QD diameter, λ is the X-ray wavelength, β is the full width at half-maximum of the peak, θ is the angle at the peak, and K is the shape factor. The ⟨110⟩ peak was used to calculate the QD diameter to eliminate complications from overlapping reflections. QD sizes and morphology were verified and the shape factor was calibrated by TEM for select samples using a JEOL-2010 microscope operated at 200 kV. The QDs were dispersed on holey carbon (400 mesh) from a toluene solution.

For thermogravimetric analysis, samples were placed into alumina crucibles for analysis on an SDT 2960 (Simultaneous DSC TGA) instrument and were heated to 300 or 600 °C at a rate of 2 °C/min under a flow of N_2 gas at 60 mL/min. Percent weight loss was determined for each sample using the accompanying TA Universal Analysis 2000 software package. A 3.5 and 5.7 nm CdSSe alloy grown from the cluster was measured by TGA at 300 and 600 °C, and the resultant powder was analyzed by XRF for S^{2-}, Se^{2-}, and Cd^{2+} content.

Solid-state ^{13}C cross-polarization magic angle spinning (CP-MAS) NMR experiments were performed at room temperature on a Varian Unity/Inova 500 MHz spectrometer with a 2.5-mm broadband MAS probe double tuned to ^1H (500.3 MHz) and the X channel to ^{13}C (125.8) MHz. A spinning speed of 12 kHz was used on all experiments. ^{13}C CP-MAS experiments were performed on $Li_4[Cd_{10}Se_4(SPh)_{16}]$, TOPO-capped CdSSe grown from $Li_4[Cd_{10}Se_4(SPh)_{16}]$, CdSe and CdSe recapped with thiophenol by ligand-exchange procedures, prepared by Cd sterate microwave synthesis. Optimum ^{13}C CP-MAS experiments were acquired using

(29) van Embden, J.; Jasieniak, J.; Gomez, D. E.; Mulvaney, P. *Aust. J. Chem.* **2007**, *60*, 457–471.
(30) Berrettini, M. G.; Braun, G.; Hu, J. G.; Strouse, G. F. *J. Am. Chem. Soc.* **2004**, *126*, 7063–7070.
(31) Dance, I. G.; Choy, A.; Scudder, M. L. *J. Am. Chem. Soc.* **1984**, *106*, 6285–6295.
(32) Choy, A.; Craig, D.; Dance, I. G.; Scudder, M. L. *J. Chem. Soc., Chem. Commun.* **1982**, 1246.
(33) Archer, P. I.; Santangelo, S. A.; Gamelin, D. R. *Nano Lett.* **2007**, *7*, 1037–1043.

an acquisition time of 50 ms, a recycling delay of 3 s, a contact time of 1.6 ms, and a ^{1}H 90° pulse length of 5 μs. ^{13}C CP-MAS buildup curves were created by varying the contact time between each experiment (0.5, 1, 1.6, 2, 2.5, and 5 ms). The chemical shifts were referenced to tetramethylsilane (0 ppm).

Synthesis of CdSSe QDs from $Li_4[Cd_{10}Se_4(SPh)_{16}]$. A series of CdSSe QDs (2−5.7 nm) were prepared from the single-source inorganic cluster $Li_4[Cd_{10}Se_4(SPh)_{16}]$ in HDA at 230 °C. QDs smaller than 2.0 nm were also prepared and isolated by carrying out the identical reaction at lower temperature (120 °C). The generic reaction was carried out in a flame-dried round-bottom flask in which 200 g of HDA was added, degassed, and placed under Ar at 70 °C for ∼1.5 h; the temperature was then raised to 120 °C. To the HDA was added 2.0 g of $Li_4[Cd_{10}Se_4(SPh)_{16}]$ (as a powder) and the reaction temperature was increased to 230 °C at an approximate rate of 1−2 °C/min. Aliquots (15 mL) were isolated every 10−20 nm based on absorption. These samples were isolated from the reaction mixture and purified using standard dissolution−precipitation protocols, in which the aliquots were solvated in toluene, methanol was added to induce precipitation, and centrifugation was done to collect the precipitate (3×). A final purification step was applied by dissolving the precipitate (20 mg) into liquid TOPO (1 g, 80 °C) for 5 min and precipitation of the QD from the TOPO using the above dissolution−precipitation procedure. TOPO exchange was utilized based upon the literature precedence implying that the surface of CdSe nanocrystals may be etched by treatment with TOPO, although no significant impact on the cation-to-anion ratio was observed.[33] The samples were stored under vacuum following isolation of the solid.

Synthesis of CdSe QDs from $Li_4[Cd_{10}Se_4(SePh)_{16}]$. A pure CdSe QD was grown from the molecular precursor $Li_4[Cd_{10}Se_4(SePh)_{16}]$ in an analogous fashion to the alloyed materials. Briefly, 40 g of HDA was added to a flame-dried round-bottom flask, degassed, and placed under Ar at 70 °C for ∼1.5 h. To the HDA was added 400 mg of $Li_4[Cd_{10}Se_4(SePh)_{16}]$ prepared by previously published methods.[33] The reaction was heated to 230 °C and monitored by absorption spectra until the desired sizes were reached. These samples were cleaned by selective precipitation with toluene/methanol, followed by TOPO exchange.

Microwave Synthesis of CdSe QDs from Cadmium Stearate (CdSA). A pure CdSe QD was grown from the reaction of cadmium stearate (CdSA) and TOPSe as described previously.[34] The reaction was carried out in decane in a CEM microwave (300 W) at 230 °C for 30 s. This sample was cleaned by selective precipitation with toluene/methanol. Size was confirmed by optical absorption and pXRD. Thiophenol was ligand-exchanged onto the CdSe surface by dissolving the CdSe sample into thiophenol, followed by sonication at ∼45 °C for 1 h.

Homogeneous Acid Etching of CdSSe QDs. Uniform etching of the crystallite faces can be accomplished with a II−VI specific etchant using 1:1 (v:v) 12 M HCl:85% H_3PO_4.[35] To etch the QD samples, the acid etchant (50−200 μL, depending on the degree of etching desired) was added to 50 mg of the CdSSe QD in excess TOPO with 1 mL of toluene and allowed to stir for ∼1 min. The solution was quenched and the etched QDs precipitated by addition of methanol. The size of the QD was verified by TEM and absorption analysis.

Results and Discussion

QD growth, whether from elemental or single-source precursors, is controlled by the nucleation and growth steps of the reaction. Growth begins with a pure nucleus (nucleation step) and can incorporate defects as the crystallite grows, depending on the concentrations and the kinetics for the specific ion addition to the growing nanocrystal surface.[36] When the single-source cluster reaction is carried out in a strongly coordinating solvent, it is presumed that QDs are generated by a mechanism similar to that proposed by Wang and Herron for formation of CdS bulk materials from $[Cd_{10}S_4(SPh)_{16}]^{4-}$.[28,37] The mechanism is believed to involve cluster coupling induced by loss of the terminal phenylthiolate, with subsequent growth occurring by a combination of cluster rearrangement into the bulk structure and S^{2-} incorporation arising from decomposition of the $[Cd(SPh)_4]^{2-}$ or SPh^- with the formation of CdS and $(Ph)_2S$ at the nanocrystal surface. In effect, the cluster has a core Cd_6S_4, and the stoichiometry is balanced in the reaction by the decomposition of the four $Cd(SPh)_4$ caps to produce six additional S^{2-} ions, six diphenyl sulfides, and four Li-SPh. The decomposition of the tetrahedral capping moieties balances the Cd:S ratio in this material.

$$Li_4[Cd_{10}S_4(Sph)_{16}] \xrightarrow{\Delta} (CdS)_{10} + 6(Ph)_2S + 4Li\text{-}SPh$$

The decomposition of phenylthiolate to produce diphenyl sulfide and S^{2-} can be mechanistically described as a simple Lewis acid-catalyzed nucleophilic aromatic substitution.[38,39] The ratio of S^{2-} incorporation from the capping moieties is controlled by the reaction temperature and conditions. In a strongly passivating solvent, QDs can be formed instead of bulk materials due to kinetic trapping by ligand passivation.[5]

For nanocrystals grown from $[Cd_{10}Se_4(SPh)_{16}]^{4-}$, the probability of S^{2-} incorporating into the growing nanocrystal with subsequent alloy formation therefore would not be surprising. The temperature of the reaction will dictate the percentage of phenylthiolate decomposition and subsequent S^{2-} content in the growing QD, while the depletion of available phenylthiolate will affect the continued incorporation into the growing QD. The nature of the resultant alloy may be a homogeneous solid solution (uniform or a gradient from core to surface),[3] a heterogeneous solid solution,[3,40] or a core−shell[10,41] material.

Highly faceted, narrow size disparity CdSSe (±<7% for 5.7 nm sample) were isolated from the single-source cluster route in the size range from 1.5 to 5.7 nm, as measured by TEM, absorption, and pXRD (Figure 2). pXRD (Figure 2D) analysis indicates that the CdSe and CdSSe QDs have wurtzite symmetry, while the CdS QDs are cubic. Control samples of pure CdSe and CdS were also isolated from single source clusters using the respective pure chalcogenide.

Elemental Distribution in the As-Prepared CdSSe. In Table 1, the Se^{2-} concentration are shown for the series of isolated CdS_xSe_{1-x} QDs grown from the single-source clusters $Li_4[Cd_{10}Se_4(SPh)_{16}]$, $Li_4[Cd_{10}S_4(SPh)_{16}]$, $Li_4[Cd_{10}Se_4(SePh)_{16}]$, CdSe passivated by TOP (CdSe-TOP), and CdSe ligand-exchanged by thiophenol (CdSe-SPh). The CdSe-TOP and CdSe-SPh QDs were grown by a microwave synthesis using cadmium stearate. It is worth noting that XRF cannot distinguish between S^{2-} incorporated into the lattice and SPh^- on the QD surface within the S^{2-}/Se^{2-} ratio, and therefore cannot distinguish between CdSSe alloy and a CdSe/CdS core−shell motif.

(34) Washington, A.; Strouse, G. *J. Am. Chem. Soc.* **2008**, *130*, 8916.
(35) Wösten, W. J. *J. Appl. Phys.* **1962**, *33*, 246–247.
(36) Bryan, J. D.; Gamelin, D. R. In *Progress in Inorganic Chemistry 54*; Karlin, K. D., Ed.; John Wiley & Sons, Inc.: Hoboken, NJ, 2005; pp 47−126.
(37) Herron, N.; Wang, Y.; Eckert, H. *J. Am. Chem. Soc.* **1990**, *112*, 1322–1326.
(38) Nose, A.; Kudo, T. *Chem. Pharm. Bull.* **1987**, *35*, 1770–1776.
(39) Takagi, K. *Chem. Lett.* **1987**, *11*, 2221–2224.
(40) Quarez, E.; Hsu, K. F.; Pcionek, R.; Frangis, N.; Polychroniadis, E. K.; Kanatzidis, M. G. *J. Am. Chem. Soc.* **2005**, *127*, 9177–9190.
(41) Peng, X. G.; Schlamp, M. C.; Kadavanich, A. V.; Alivisatos, A. P. *J. Am. Chem. Soc.* **1997**, *119*, 7019–7029.

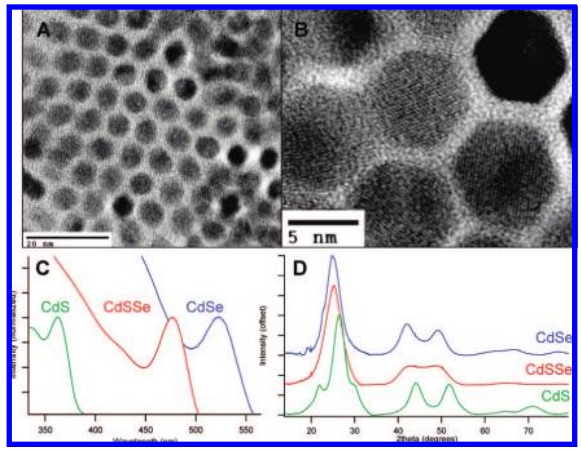

Figure 2. (A) TEM image of 5.7 nm CdSSe QDs with a S^{2-}:Se^{2-} ratio of 66:34 by XRF. (B) HRTEM images of the same sample with visible lattice fringes. (C) Absorption spectra of ~2.4 nm CdSe, CdSSe, and CdS QDs. CdSSe QD S^{2-}:Se^{2-} is 36:64 by XRF. (D) pXRD spectra of ~2.4 nm QD samples.

Although many microanalytical techniques can be used to evaluate S^{2-} content, XRF is the most accurate for analyzing the S^{2-}:Se^{2-} ratios, as there are no complications from overlapping peaks as observed in XPS[42,43] (Supplemental Figure 1, Supporting Information).

Inspection of Table 1 indicates that, for the five individual reactions for formation of the CdSSe QDs (four at 230 °C and one at 120 °C), an increase in S^{2-} content is observed as the QDs increase in size up to ~3.5 nm, where the S^{2-}/Se^{2-} ratio approaches an asymptote at ~60% sulfur. The S^{2-} content in CdSe-TOP (3.1 nm) is 0%. Upon ligand-exchange with thiophenol, the S^{2-} content for the 3.1 nm CdSe-SPh is 51%. The marked increase in S^{2-} implies that a significant fraction may arise from contributions of phenylthiolate bound to the surface and S^{2-} incorporated into the QD. In all the CdSSe samples in Table 1, a high concentration of S^{2-} is observed, although for a reaction temperature of 120 °C, the S^{2-} content is suppressed, presumably due to the reduced thiophenolate decomposition at lowered reaction temperatures resulting in less S^{2-} available for incorporation.

To rationalize the S^{2-} content observed in the CdSSe alloys and the CdSe-SPh sample, the presence or absence of phenylthiolates at the QD surface must be established. The presence of phenylthiolate bound to a QD surface will substantially modify the actual S^{2-} content measured in a QD sample, resulting in a significant skewing of the XRF results and thus an incorrect conclusion about the material motif.

To analyze the surface of the prepared CdSSe and CdSe QDs, CP-MAS solid-state NMR experiments were performed on one of the CdSSe growth reactions to help determine the nature of the ligands bound to the surface of the QDs. The CP-MAS data in Figure 3 shows the carbon signatures of the organic surface ligands for the aromatic resonances arising from SPh^-, aliphatic signatures arising from TOPO, TOPSe, and stearic acid, and the −COOH signature from stearic acid. The aromatic resonances of $Li_4[Cd_{10}Se_4(SPh)_{16}]$ (Figure 3A) can be assigned as 137.49 (alpha), 134.57 (ortho), 127.17 (meta), and 123.32 ppm (para), and the signatures at 9 and 46 ppm can be assigned to impurities from triethylamine. The CdSSe QDs grown from $Li_4[Cd_{10}Se_4(SPh)_{16}]$ (Figure 3B−G) are consistent with the assignments for thiophenol bound to the QD surface. The aliphatic signatures for the CdSSe cluster are observed between 10 and 40 ppm and can be assigned as contributions arising from TOPO, consistent with the observed resonances for TOPO in Figure 3J. For the 3.2 nm CdSSe QD (Figure 3D), the line width appears to increase dramatically, which may arise from chemical shift anisotropy between different sites on the CdSSe QD surface. This conclusion is reasonable, as the highest phenylthiolate concentration relative to TOPO is observed at this size.

NMR assignments for the CdSe-TOP QD (3.1 nm) grown from CdSA (Figure 3H) show contributions from the −COOH feature (180 ppm), assignable to stearic acid (Figure 3K). In addition, the aliphatic region consists of contributions from

Table 1. Experimental Results for S^{2-}/Se^{2-} Composition, QD Diameter by Scherrer Broadening of the ⟨110⟩ pXRD Reflection, and Exciton Absorption ($1s_e - 1s_h$)

	XRF % [Se][a]	eff. mass appox. % [Se][b]	abs. λ (nm)	XRD (Scherrer) diameter (nm)[c]
CdSSe	64	78	477	2.44
(230 °C)	69	76	502	2.93
	77	81	511	3.03
Growth 1	67	77	517	3.16
	58	77	522	3.26
Growth 2	58	89	457	1.96
	75	90	489	2.32
	85	87	498	2.56
	66	76	507	2.97
	60	74	516	3.26
	37	78	560	4.42
	36	78	567	4.71
Growth 3	52	70	473	2.57
	60	77	488	2.64
	61	71	497	2.96
	58	78	509	2.97
	55	77	514	3.10
	36	78	539	3.65
	35	81	548	3.81
	36	82	564	4.30
	39	73	567	5.13 [5.09]
	34	69	570	5.74 [5.78]
SSNMR	–	85	463	2.08
Growth 4	–	76	499	2.80
	–	68	505	3.23
	–	73	529	3.64
	–	74	546	4.06
	–	67	567	5.68
CdSSe	88	99	430	1.56
(120 °C)	77	81	450	2.05
	76	79	466	2.25
	74	84	486	2.40
CdSe	100	100	498	2.22
	100	100	519	2.46
	100	100	526	2.65
	100	100	532	2.77
CdSe-TOP[d]	100	100	544	3.10
CdSe-SPh[d]	49	100	544	3.10
CdS	0	0	352	2.41

[a] %[Se]/([Se] + [S]) measured by XRF. [b] %[Se] calculated by the effective mass approximation. [c] Bracketed numbers are diameters verified by HRTEM. [d] Synthesized via cadmium stearate microwave synthesis.

(42) Bowen Katari, J. E.; Colvin, V. L.; Alivisatos, A. P. *J. Phys. Chem.* **1994**, *98*, 4109–4117.
(43) Bae, W. K.; Char, K.; Hur, H.; Lee, S. *Chem. Mater.* **2008**, *20*, 531–539.

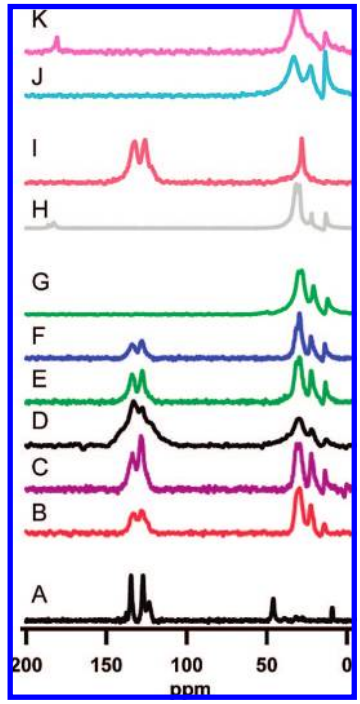

Figure 3. Solid-state ^{13}C CP-MAS NMR of (A) $Li_4[Cd_{10}Se_4(SPh)_{16}]$, (B) 2.1 nm CdSSe, (C) 2.8 nm CdSSe, (D) 3.2 nm CdSSe, (E) 3.6 nm CdSSe, (F) 4.1 nm CdSSe, (G) 5.5 nm CdSSe, (H) 3.1 nm CdSe grown from CdSA synthesis, (I) 3.1 nm CdSe (CdSA grown) capped with thiophenol, (J) trioctylphoshphine oxide, and (K) stearic acid.

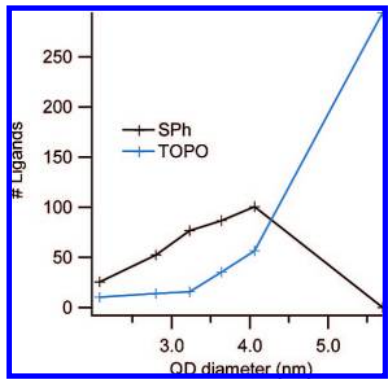

Figure 4. Number of ligands bound to CdSSe QDs plotted vs QD diameter. Percent of ligands was determined semiquantitatively by ^{13}C CP-MAS NMR.

stearic acid and TOP in the 10−40 ppm range. CdSe-TOP QD was ligand-exchanged with thiophenol, which results in complete loss of the stearic acid signature (180 ppm) and the predominant aliphatic contributions (10−40 ppm). In the aromatic region the signature for thiophenol is clearly present (Figure 3I) for CdSe-SPh.

Integrations of the aromatic and aliphatic regions of Figure 3B−G reveal the relative ratio of ligands bound to the surface of the QD as it grows from 2.1 to 5.7 nm. Using these ratios, the number of SPh^- and TOPO ligands were determined, and are plotted in Figure 4. The loss of the resonance for thiophenol (Figure 3G) for the 5.7 nm QD was confirmed on replicate measurements on QD samples between 5 and 5.7 nm in size. The concentration of thiophenol to aliphatic can be evaluated semiquantitatively using ^{13}C CP-MAS NMR signals. ^{13}C CP-MAS experiments were chosen over ^{13}C MAS to determine the relative ratio of SPh:TOPO due to the improvement in signal-to-noise ratio, faster experiment collection times, and because ^{13}C and ^{1}H are only present as surface ligands; therefore the cross-polarization should have a minimal effect on signal intensity. To ensure that signal intensities were not affected and T_1 relaxation was allowed to fully recover, a series of MAS experiments were performed where the recycle delay was varied (3, 6, 10, and 20 s), and the optimum recycle delay was determined to be 10 s. A comparison was made between the intensity ratios for the CP-MAS and MAS experiments to validate that the CP-MAS experiment did not skew the reported ratios. Assuming the alkane passivant is predominately TOPO, the relative ratio from the MAS experiment was 1 TOPO:6 SPh^-, while the CP-MAS had a ratio of 1:5.8. Although the T_1 for the ^{13}C signal was not measured, the agreement in CP-MAS and MAS measurements at 10 and 20 s delay suggests that the analysis is fairly accurate. Buildup curves were also performed to ensure that $T_{1\text{-Rho}}$ was not compromised and the ^{13}C signal was allowed to fully recover (Supplemental Figure 2, Supporting Information).

The plot of the number of ligands versus size is intriguing, as it suggests that the phenylthiolate content increases with increasing size up to 4 nm and then decreases as the QD continues to grow. Ligand-exchange by TOPO, pyridine, or HDA does not modify the observed phenylthiolate concentration ratio in these materials. This observation is consistent with our earlier publication,[30] where the phenylthiolate was observed to be remarkable robust on the QD surface, exhibiting a lack of exchange by pyridine at 70 °C or TOPO at 80 °C.

The difference in the phenylthiolate concentration between small (3.5 nm) and large (5.7 nm) CdSSe samples is further evidenced by analyzing TGA data for these materials. TGA on 3.5 and 5.7 nm CdSSe exhibits marked differences for ligand loss at 600 °C. The mass loss at 600 °C is assignable to thermal degradation of two SPh^- ligands with production of a free S^{2-} and diphenyl sulfide, as observed in the earlier TGA studies by Wang and Herron.[28] The smaller QD shows significant loss of S^{2-} associated with ligand loss at 600 °C (42% → 21%), while the 5.7 nm QD shows insignificant changes in S^{2-} (66% → 63%) when heated to 600 °C. The lower loss for S^{2-} corroborates the lack of SPh^- on the QD surfaces, as observed in the NMR data.

The NMR data and TGA analysis conclusively show that SPh^- is present in these materials for sizes below 5 nm and is a contributor to the observed S^{2-} in XRF. It is important, therefore, to note that the total S^{2-} content reported in Table 1 will be artificially high; however, the observation of ~60% S^{2-} content above 3.5 nm, where SPh^- coverage is dropping, cannot be attributed solely to SPh^-, particularly for the 5.5 nm QD where no SPh^- is experimentally observed. Although a core−shell motif could explain this observation, our ^{77}Se CP-MAS data at short contact times from earlier studies clearly demonstrate Se^{2-} at the surface by $^{1}H-^{77}Se$ CP-MAS experiments.[30] This result has been confirmed for all sizes in this study (unpublished) and is currently being analyzed. To properly project the CdSSe composition and thus the elemental distribution, the quantity and characteristics of SPh^- at the QD surface must be better understood and analyzed.

Nature of the CdSSe Alloy. While the presence of SPh^- on the QD surface could rule out a simple core−shell motif to explain the S^{2-} enrichment, it does not rule out S^{2-} ion incorporation into the growing QD. The actual nature of the alloy formed during the reaction, whether homogeneous or inhomogeneous, is still unknown (Figure 1). Insight into the

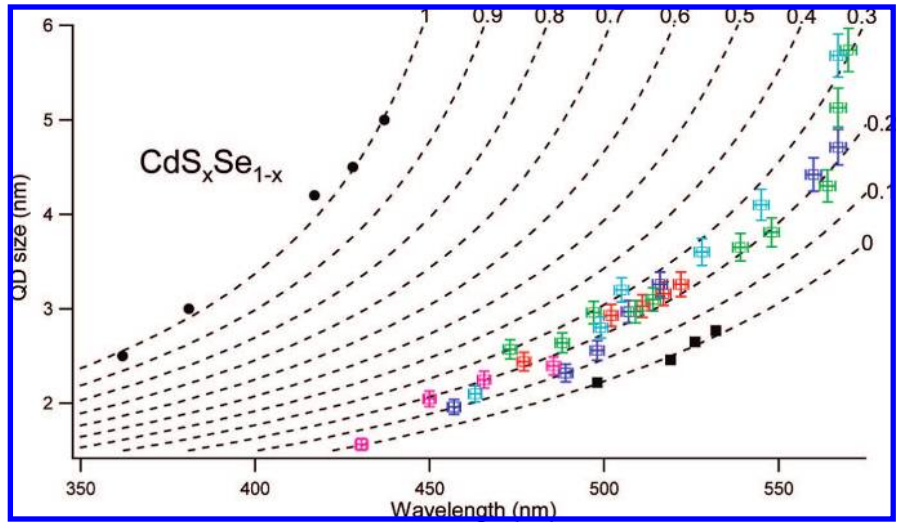

Figure 5. Five separate CdSSe QD reactions grown from $Li_4[Cd_{10}Se_4(SPh)_{16}]$. Sizes measured by pXRD Scherrer−Debye analysis and calibrated by HRTEM. Dashed lines are theoretical EMA of the indicated concentrations of S:Se. Squares are pure CdSe QD samples. Circles are pure CdS QD samples from ref 43.

nature of the alloy may be gained by considering the impact of formation of a solid solution on the electronic properties of the semiconductor QD, using EMA to account for the tuning of the semiconductor band gap by the alloying of the ternary ion. The change in the exciton absorption as a function of size and composition can be generated by use of the theoretical model described by Rosenthal et al.[3] for CdSSe QD homogeneous alloys. By applying the size-dependent confinement formula of the EMA (eq 2) and utilizing known energy shifts for pure cluster grown samples,[44] an expression can be generated for the shift in the exciton as a function of elemental composition,

$$E_g(x,d) = x\left[E_g(\mathrm{CdS},\infty) + \frac{a_1}{d} + \frac{c_1}{d^2}\right] + (1-x)\left[E_g(\mathrm{CdSe},\infty) + \frac{a_2}{d} + \frac{c_2}{d^2}\right] - b(d)x(1-x) \quad (2)$$

where a and c represent the reduced masses of the e^- and h^+ (fit as empirical parameters), d is the QD diameter, and b is the bowing constant describing the nonlinear effects of ion-doping.

Figure 5 shows the change in the energy for the first exciton absorption for the five individual reactions for CdS_xSe_{1-x} QDs. The experimental data are overlaid with theoretical plots calculated by EMA. Inspection of the absorption value for the exciton versus the measured size shows that there is a shift in the energy gap when compared to pure CdSe or CdS QDs of the same size. The first excitonic transition exhibits a blue shift of 41 nm for a QD of the same size (Figure 2C). The core−shell motif, where CdSe and CdS phases are completely segregated, does induce a shift in the absorption edge but has a much weaker (~8 times less) effect at low dopant concentrations.[3,41] The observed shift in the first exciton transition of CdSSe relative to CdS and CdSe QDs provides direct and conclusive evidence of S^{2-} incorporation into the lattice. Although the effective mass equation is an approximation for describing the QD absorption properties, the experimental plots support a homogeneous alloy formation. The details of the alloy, whether uniform or a gradient from core to surface, are not defined by the absorption data alone, and only correlation of all the experiments can provide a map of the formed alloy.

Qualitative Model of the QD. Using a model for the alloy growth based upon the initial observations of Wang and Herron[28] for growth of CdS from $Li_4[Cd_{10}S_4(SPh)_{16}]$, one might suspect the final composition of a QD grown from $Li_4[Cd_{10}Se_4(SPh)_{16}]$ to exhibit a ratio of 60% S^{2-} and 40% Se^{2-}. This can be deduced on the basis of stoichiometry, where the composition is 10 Cd^{2+} to 4 Se^{2-} to 6 S^{2-} (from SPh^-) and the remaining products consist of six $(Ph)_2S$ and four Li-SPh. The actual stoichiometry will be further enriched in S^{2-} if the remnant four Li-SPh further decompose at the QD surface. The additional S^{2-} generated by this decomposition would result in 66% S^{2-} arising from the phenylthiolate decomposition, and a ratio of ~1:1.2 Cd:chalcogenide. While decomposition of phenylthiolate is critical, this is a temperature-dependent reaction, and at the initial reaction temperatures, crystallization theory[36] should dominate, with a pure nucleus forming first. As the temperature of the reaction increases, phenylthiolate decomposition will increase, roughly proportional to the available surface area above a critical temperature, leading to what one might suspect will be an enrichment of S^{2-} approaching the 60% reaction stoichiometry of the cluster. In the growth of CdSSe QDs from $[Cd_{10}Se_4(SPh)_{16}]^{4-}$, the reaction will be complex, dominated by the decomposition mechanism, which is temperature-dependent, the concentration of surface-bound phenylthiolate, and the rate of S^{2-} incorporation versus Se^{2-} incorporation, since the rate of atom addition is dictated by the reactivity of the QD surface.

Evidence of the model can be generated by inspection of the Cd:chalcogenide ratio for the QDs from XRF compared to the change in the S^{2-} content estimated by EMA. Measuring the S^{2-} content by EMA and XRF provides insight into the average composition relative to the total S^{2-} composition as a function of the QD size. The Cd:chalcogenide ratio is approximately 1:1.1 (Cd:S + Se) across all samples, indicative of an anion-rich surface. Plots of the percentage [Se] and [S] extracted by the EMA and by XRF versus size for the growth reactions are combined and shown in Figure 6. The S^{2-} content calculated from the EMA, which correlates with band gap tuning arising from alloying, exhibits a slow increase (22−31%) with increas-

(44) Khitrov, G. A. Thesis, University of California, Santa Barbara, 2003.
(45) Hiemenz, P. C. *Polymer Chemistry: The Basic Concepts*; Marcel Dekker, Inc.: New York, NY, 1984; pp 423−504.

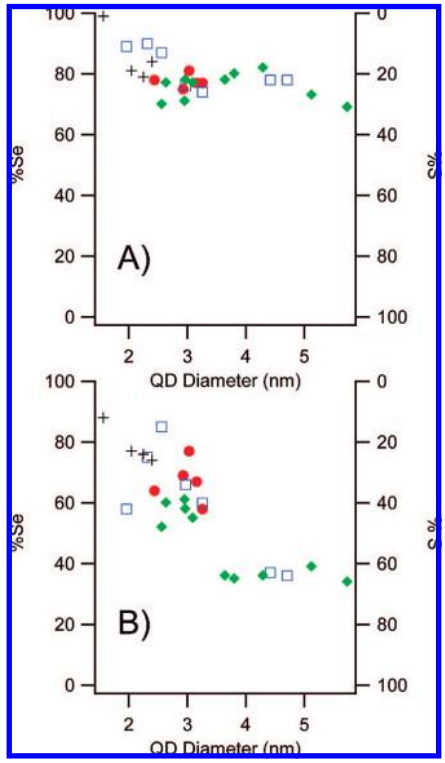

Figure 6. (A) CdSSe concentrations calculated by effective mass approximation, plotted against QD size. (B) CdSSe concentrations calculated by XRF, plotted against QD size.

ing QD size (3.65−5.9 nm). The exception is the 1.5 nm QD, where only 1% S^{2-} incorporation is observed, consistent with the presence of only SPh^- and not the alloying of S^{2-}. The observation of insiginificant S^{2-} incorporation in this size regime is indicative of a pure nucleus, as predicted by nucleation theory. Efforts by Gamelin et al. have pointed toward the critical nuclei for CdSe to be roughly 1−2 nm in size, in agreement with our observation.[36]

The change in S^{2-} content for the XRF data is more dramatic. At sizes below 3.2 nm, the S^{2-} content is varied with a composition of 15−40%. Above 3.2 nm, the S^{2-} content exhibits a discontinuity with values of ∼60% S^{2-}. The XRF data are influenced significantly at small sizes by surface contributions from bound phenylthiolate based purely upon surface-to-core ratios for the QDs. As the QD grows, the surface contribution to total S^{2-} content will become less significant. The marked increase for S^{2-} in the XRF above 3.2 nm, but with no significant jump in the EMA data, implies that increased phenylthiolate decomposition is occurring at the QD surface, resulting in increased S^{2-} content. Coupling this result with the stoichiometric expectations for the QD growth from a cluster, 60% incorporation is consistent.

To evaluate the jump in S^{2-} arising from increased phenylthiolate decomposition, Figures 4 and 6 are compared. In Figure 4, the NMR data, which track phenylthiolate and alkane ligands at the surface of the QD, show a maximum phenylthiolate content at ∼4 nm, dropping to nonmeasurable levels above 5 nm for CdSSe QDs. If we consider the fact that the sulfur incorporation is a complex issue of temperature, and the available surface area of the QD for phenylthiolate decomposition, the decrease in phenylthiolate in the NMR below 4 nm can be accounted for by enhanced phenylthiolate decomposition, resulting in S^{2-} incorporation. The assumption that S^{2-} incorporation is influenced by reaction temperature is clearly seen in Table 1, where lower sulfur content is observed for reactions carried out at lower reaction temperatures (120 °C). The nearly invariant composition in the EMA coupled to the stepped increase in XRF reflects the gradient nature of the alloy due to the complex reaction pathway for QD growth from clusters coupled to contributions from enhanced decomposition rates and potentially changes in surface energy of the growing QD. The loss of phenylthiolate from the QD surface and increased S^{2-} content at the largest sizes can be supported by the broadening of the absorption feature for the first exciton (Supplemental Figure 3, Supporting Information). The broadening of the absorption feature is partially due to a loss of distribution, as shown in the TEM image (∼7%), but is also likely due to the apparent discontinuity in the S incorporation in these sizes.

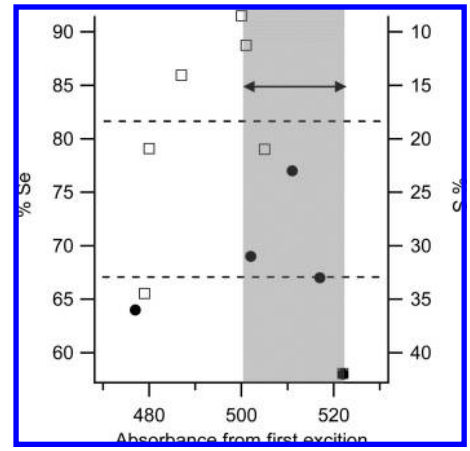

Figure 7. The %Se (and %S) from XRF analysis from a 3.26 nm CdSSe QD, taken during growth (circles) and then subsequent acid-etching (squares) by H_3PO_4/HCl (50% v:v). The shaded area represents removal of ∼0.4 nm, approximately one lattice plane.

To support the conclusion that S^{2-} is incorporated into the growing alloy for QDs below 5 nm, a 3.26 nm CdSSe QD was analyzed for S^{2-} content during growth and subsequent etching with a II−VI acid etchant (H_3PO_4/HCl). A similar approach to etching has been carried out by Peng et al.[46] In Figure 7, the experimental data show that the S^{2-} contents in both the growing and etched QDs track nearly perfectly for removal of a single shell from the QD, and this is observed to reproduce the ion content at the smallest size. The lack of agreement is consistent with the probability that etching is not uniform for all faces. The remarkable observation is the rapid decrease in S^{2-} content for the first shell removal.

Comparing this observation to the NMR data, which indicates the presence of phenylthiolate, allows the conclusion that the high S^{2-} content is due primarily to the presence of phenylthiolate and not core shelling. Removal of approximately two shells from the QD yields a value for S^{2-} between those for the grown and etched samples determined by XRF. The remarkable correlation between the etching experiment (Figure 7), the Se^{2-} concentration as a function of size measured by the EMA (Figure 6A), and the increased S^{2-} incorporation reflected in NMR and XRF (Figure 4 and 6B) supports the conclusion that

(46) Lu, W. W.; Qu, L.; Guo, W.; Peng, X. *Chem. Mater.* **2003**, *15*, 2854–2860.

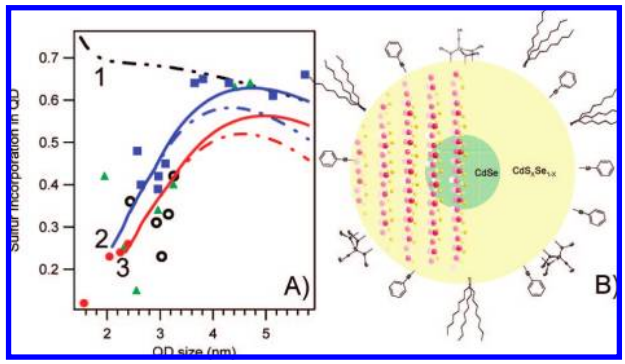

Figure 8. (A) Sulfur incorporation vs QD size. Line 1 depicts growth of a uniform 60S/40Se alloy. Line 2 depicts growth of a 2 nm pure CdSe core with 70S/30Se (solid) and 60S/40Se (dashed). Line 3 depicts growth of a 2.25 nm pure CdSe core with 70S/30Se (solid) and 60S/40Se (dashed). Other points are experimental growth reactions determined by XRF. (B) Model of a CdSSe QD, showing crystal structure with organic ligands passivating the surface. CdSSe QD cross-section is cut on the ⟨110⟩. Model depicts pure CdSe nucleus with CdSSe alloy.

an alloy is formed in the reaction and phenylthiolate is the major contributor of the apparently high S^{2-} concentration.

Conclusion

The nature of and ion distribution within the CdSSe QD alloy requires a model that can account for the experimentally derived S^{2-} composition by XRF (Figure 6), the postulation of a pure core (∼1.5−2 nm), and the S^{2-} contributions arising from surface-bound phenylthiolate contributions, as observed in Figure 4. In Figure 8, a plot of the fractional S^{2-} composition as a function of QD size is shown. The experimental XRF data from four separate reactions are plotted. Assuming the cluster stoichiometry of 60% S^{2-} arising from phenylthiolate decomposition and contributions from bound phenylthiolate based on the NMR results yields the black line (line 1). Although the agreement is reasonable for QDs >4 nm, the lack of agreement with experimental data below 4 nm suggests the QD is not a uniform alloy. Incorporating a pure CdSe nucleus, as suggested by nucleation theory, yields lines 2 and 3 (blue and red), where a 2 (blue) and 2.25 nm (red) pure CdSe core is assumed and subsequent 60:40 (dashed) and 70:30 (solid) S^{2-}-to-Se^{2-} incorporation arises as the QD grows. Inclusion of a pure core gives surprisingly good agreement with the experimental data for a 2 nm core with an alloy at 70:30 S^{2-}: Se^{2-}. The theoretical plots were generated by predicting the number of atoms on the basis of the sizes and number of SPh^-, determined by ^{13}C CP-MAS NMR. A number of assumptions are made in the generation of these plots, such as uniform growth, no defect sites, and 100% surface passivation by ligands based on available binding sites.

Although the data below 4 nm are scattered, suggesting a rather complex reaction, the agreement suggests a model where a pure nucleus is generated and S^{2-} addition reaches equilibrium above 4 nm (Figure 8A). The complexity of the reaction arises from the different rates of S^{2-} production from SPh^- decomposition, increases in reaction temperature, and rates of S^{2-} incorporation in the growing QD. It is believed that the S^{2-} incorporation rate becomes more uniform as the observed phenylthiolate concentration bound to the QD drops, presumably reflecting near-instantaneous degradation upon phenylthiolate adsorption on the QD surface.

Taking the complete data set, a model (Figure 8B) can be proposed for the CdSSe alloy grown from the molecular cluster. At the core, a pure CdSe nucleus of ∼1.5 nm exists with phenylthiolate bound to the QD surface. As the particle grows, the reaction temperature, surface area, and phenylthiolate decomposition rate increase; likewise, the level of S^{2-} alloying increases. At the largest sizes, loss of phenylthiolate, verified from the CP-MAS, but continued incorporation of S^{2-} are observed, supporting the increased decomposition rate and implying that a constant S^{2-} rate should be observed reflecting anion availability and the thermodynamics of the reaction. The rate of incorporation approaches the stoichiometric value determined by XRF, and an increasing alloy composition is indicated by EMA. The slow increase in EMA reflects the slow rate of alloy formation in the core of the QD relative to the outermost shells.

The data support a model where the Se^{2-} is not restricted to the core and the S^{2-} is not restricted to the surface, as expected for a core−shell, but rather represents a solid solution whose composition is controlled by thermodynamic parameters, namely S^{2-} concentration, energetics of S^{2-} versus Se^{2-} addition to a growing QD, and the conversion from a kinetically controlled reaction to a thermodynamically equilibrated process. It is not surprising that the compositional distribution of the S^{2-} in the CdSSe QDs approaches the stoichiometric value of 60%, but the mechanism is quite complex if one considers the implications of nucleation theory and the influence of the precursor concentrations on the kinetics as the reaction progresses, since the available reactant concentrations (S^{2-} vs Se^{2-} vs Cd^{2+}) are in constant flux.

Acknowledgment. The authors acknowledge financial support of the project through the National Institutes of Health (NBIB 7 R01 EB000832) and the National Science Foundation (DMR-0701462). The TEM images were measured at the National High Magnetic Field Laboratory at Florida State University (NSF DMR-9625692) with the assistance of Dr. Yan Xin. The solid-state NMR measurements were performed at the Florida State University Chemistry Department NMR facility with the assistance of Dr. Randall Achey.

Supporting Information Available: XRF spectra of Cd^{2+}, Se^{2-}, and S^{2-} with labeled peaks (Supplemental Figure 1); ^{13}C CP-MAS buildup curves for 3.6 nm CdSSe QD (Supplemental Figure 2); and absorbance profile for a growing CdSSe QD from $Li_4[Cd_{10}Se_4(SPh)_{16}]$ (Supplemental Figure 3). This material is available free of charge via the Internet http://pubs.acs.org.

JA805453S